

Free Energy Manifold: Score-Based Inference for Hybrid Bayesian Networks

Cheol Young Park¹, Shou Matsumoto²

¹ATOS Co., Ltd., 273, Digital-ro, Guro-gu, Seoul, 08381, Republic of Korea

²C5I Center, George Mason University, Fairfax, VA 22030, USA
cparkf@gmu.edu, smatsum2@masonlive.gmu.edu

Abstract

The Free Energy Manifold (FEM) builds on conditional energy-based and score-based density estimation, and *specializes* them as composable inference factors for hybrid Bayesian networks (BNs) — not as a new generic conditional density estimator. Concretely, FEM is a score-trained conditional energy network $E_\theta(z_X^k, y, \sigma)$ that serves *four* inference roles within a single learned object: (i) discrete posterior $P(X | y)$; (ii) generative sampling $P(Y | X=x)$ via annealed Langevin; (iii) multi-leaf composition by energy addition under conditional independence (CI), with a shared joint form for CI-violating leaves; and (iv) sparse-data inference over high-cardinality discrete parents through learned prototype embeddings, in place of an explicit $K^{|Pa|}$ table.

We identify and analyze a *mode-bridge artifact*, a posterior calibration failure that, to our knowledge, has not been previously characterized in the score-based or hybrid-BN literature: multilayer perceptron (MLP) smoothness produces a low-energy ridge between modes *of the same class*, yielding over-confidence at off-distribution interior points. A simple *valley regularization* addresses this, and we characterize the optimal strength $\lambda^*(D)$ as a non-monotonic three-phase landscape driven by cross-class energy gap (linear in D), softmax saturation (exponential in ΔE), and mode-conflict probability (low- D suppression).

On our synthetic anti-correlated multimodal hybrid-Bayesian network benchmarks, FEM achieves 60–172 \times lower Kullback–Leibler (KL) divergence than the best non-FEM baseline at the canonical $D=5$ setup (vs. conditional linear Gaussian (CLG), kernel density estimation (KDE), KDE-product, and histogram-product) and 3.6–770 \times lower midpoint KL than a conditional energy-based model (CEBM) across our (D , mode-scale) generality grid (9 cells, 2–3 seeds per cell); 8.1 \times at $K^M=6,561$ parents, with a real-data sanity check showing 2.7 \times better negative log-likelihood (NLL) than CLG on UCI Breast Cancer ($D=30$). In a 4-seed head-to-head against the canonical conditional EBM ($\lambda=0$ FEM) and a Mixture Density Network (MDN) baseline on a $D=5$ bimodal benchmark, FEM is 300 \times better than CEBM and 122 \times better than MDN at the mode-bridge midpoint, isolating valley regularization as the Bayesian network-inference-targeted fix. In a multi-leaf compositional benchmark ($X \rightarrow Y_1, Y_2, Y_3$), FEM uses a *single* trained energy factor to handle all 7 non-empty evidence patterns and beats per-pattern MLPs by 5.3 \times at the full-evidence boundary query despite MLPs training 7 \times as many models, directly evidencing FEM as a composable Bayesian network inference factor rather

than a fixed-pattern classifier. On pure-classification benchmarks (MNIST), a discriminative MLP retains a sizable accuracy lead, consistent with the generative-vs-discriminative paradigm distinction we discuss in Section 7. FEM’s novelty thus lies not in using an energy function for conditional density estimation *per se*, but in the Bayesian network-compatible inference semantics, compositional use across continuous leaves, and the identification and correction of the mode-bridge artifact.

1 Introduction

Inference in Bayesian networks with mixed discrete/continuous variables is foundational to probabilistic reasoning, yet remains challenging when (a) multiple continuous leaves share a discrete parent and must be *jointly* integrated, (b) hidden confounders break conditional independence, (c) $K^{|Pa|}$ exceeds available data, or (d) continuous evidence requires *sampling* posteriors rather than just evaluating them.

Standard tools fail in characteristic ways. Conditional Linear-Gaussian (Lauritzen 1992) cannot represent multimodality; Histogram-Bayesian network and Neural CPT suffer K^M table explosion; Kernel Density Estimation suffers the curse of dimensionality (Silverman 1986). Score-based generative modeling (Song and Ermon 2019) offers a parametric alternative whose energy network scales *linearly* with D .

We propose the **Free Energy Manifold** (FEM), an NCSN-style energy network $E_\theta(z_X, y, \sigma)$ over learned discrete-parent embeddings z_X^k and continuous evidence $y \in \mathbb{R}^D$. Our contributions:

1. **Bayesian network-compatible score-based energy factor** (Section 3). We formulate a score-trained conditional energy model as a hybrid-Bayesian network factor over discrete parents and continuous children, enabling posterior inference $P(X | y)$ and generative sampling $P(Y | X=x)$ from the same learned object. The novelty here is the Bayesian network-compatible inference semantics, not the use of an energy function for conditional density estimation *per se*.
2. **Composable inference** (Section 3, Section 6). We exploit the additive structure of energies to implement Bayesian network likelihood composition: conditionally

independent continuous leaves combine by energy addition, while CI-violating leaves are absorbed by a shared joint FEM. This *compositional use* of conditional EBMs across multiple continuous leaves of a hybrid Bayesian network is the inference-factor setting we systematically study and benchmark.

3. **Scalable discrete-parent representation** (Section 3, Section 6). We replace explicit $K^{|\text{Pa}|}$ conditional tables with learned discrete-parent prototype embeddings, improving generalization in sparse high-cardinality parent configurations.
4. **Mode-bridge artifact and valley regularization** (Section 4, Section 5). We identify a posterior calibration failure mode of smooth neural energy factors on multimodal classes and propose a single off-data uniform-posterior regularizer that suppresses the spurious inter-mode bridge. We further decompose the optimal strength $\lambda^*(D)$ into a non-monotonic three-phase landscape driven by cross-class gap (linear in D), softmax saturation (exponential in ΔE), and mode-conflict probability (low- D suppression). We provide an explicit characterization of this artifact and the corresponding mitigation in the score-based hybrid-Bayesian network setting.
5. **Empirical characterization and scope-honest limits** (Section 6, Section 7). On synthetic anti-correlated multimodal hybrid-Bayesian network benchmarks, FEM obtains 60–172 \times best non-FEM KL at the canonical $D=5$ setup (vs. CLG/KDE/KDE-product/Hist-product) and 2.7 \times better NLL on UCI Breast Cancer ($D=30$). In a 4-seed head-to-head against the canonical conditional EBM and a Mixture Density Network baseline (Section 6.7), FEM is 300 \times better than CEBM and 122 \times better than MDN at the mode-bridge midpoint, isolating valley regularization as the Bayesian network-inference-targeted contribution. In a multi-leaf compositional benchmark with three CI leaves (Section 6.8), FEM uses a single trained factor to handle all 7 evidence patterns and beats per-pattern discriminative MLPs by 5.3 \times on the full-evidence boundary query despite MLPs training 7 \times more models — direct evidence of FEM-as-inference-factor. A (D , mode-scale) generality sweep (Section 6.9) confirms FEM-vs-CEBM advantage in 9/9 cells (ratio 3.6 \times to 770 \times), and a $K_X \in \{3, 5, 7\}$ axis sweep extends the result to multi-bimodal class layouts (3/3 cells, 25 \times to 770 \times), while exposing a high- D residual artifact and mild $K_X=7$ in-data degradation as honest limitations. On pure-classification benchmarks (MNIST), a discriminative MLP retains a sizable accuracy advantage, framing FEM as a probabilistic-inference complement rather than a classifier replacement.

Positioning. We view FEM through a *closed-world vs. open-world* paradigm distinction. *Closed-world classification* — predicting a fixed Y from a fully observed X — is the natural domain of discriminative models (MLP, CNN, Transformer), which optimize $P(Y | X)$ directly with no capacity wasted on irrelevant joint structure. *Open-world probabilistic inference* — handling missing observations,

generative scenarios, hidden confounders, mode multiplicity, and inverse problems over multi-leaf BNs — is fundamentally different: each new query type would require a new discriminative model, yet the joint distribution remains unique. FEM, as a hybrid probabilistic graphical model, addresses all such queries through a single energy network. We do not propose FEM as a competitor to MLP on closed-world benchmarks; we propose it as the missing complement for the open-world inference space where current hybrid Bayesian network tools (CLG, KDE, Histogram-Bayesian network, Neural CPT) exhibit limitations in the regimes we study.

2 Background and Related Work

2.1 Hybrid Bayesian Networks

A hybrid Bayesian network over discrete X and continuous Y specifies $P(X, Y)$ via factors mixing categorical and continuous variables; posterior inference $P(X | y_{\text{obs}})$ requires per-class likelihoods. CLG (Lauritzen 1992; Lauritzen and Jensen 2001) provides closed-form posteriors when each conditional $Y | X=k$ is a single Gaussian — correct only for unimodal classes. Mixtures of truncated exponentials (Moral, Rumí, and Salmerón 2001; Cobb and Shenoy 2006) and mixtures of polynomials (Shenoy and West 2011) extend expressivity but require manually specifying the mixture form. The recent Salmerón et al. (2018); Langseth et al. (2009) surveys enumerate particle, sampling, dynamic discretization, and junction-tree variants; all share difficulty in $D \gg 5$ where the underlying density estimators degrade. Histogram-Bayesian network with Laplace smoothing and KDE-Bayesian network (Silverman 1986; Wasserman 2006) are common non-parametric baselines but suffer $K^{|\text{Pa}|}$ explosion or bandwidth-induced failure (Section 6). Neural CPT parameterizes $P(Y_{\text{bin}} | X)$ via shared MLPs; FEM extends this to fully continuous Y . We position FEM as a *parametric* alternative whose energy network has $\mathcal{O}(D \cdot \text{hidden})$ parameters regardless of $K^{|\text{Pa}|}$, learns smooth densities without manual mixture specification, and *instantiates score-based energy learning as a reusable inference factor inside hybrid Bayesian networks* — not just as another conditional density estimator.

2.2 Score Matching and Energy-Based Models

Score matching (Hyvärinen 2005) and denoising score matching (DSM) (Vincent 2011) estimate $\nabla \log p$ consistently without the intractable partition function. NCSN (Song and Ermon 2019) introduces σ -conditional score networks $s_\theta(z, \sigma)$ and annealed Langevin sampling, preventing the mode collapse that besets naive Langevin on multimodal targets — directly inspiring FEM. Score-SDE (Song et al. 2021) and DDPM (Ho, Jain, and Abbeel 2020) extend to time-continuous and discrete-step diffusion. Energy-based modelling more broadly (LeCun et al. 2006; Du and Mordatch 2019) grounds the conceptual framework but typically does not address discrete-conditional posterior inference. The closest precursor to FEM is NCSN; we add (i) learned discrete prototypes μ_X^k , (ii) a CE anchor specialized

for discrete-given-continuous queries, and (iii) valley regularization.

2.3 Neural Conditional Density Estimation and Conditional EBMs

FEM is, by construction, a conditional energy-based model: it parameterizes $p_\theta(y | x) \propto \exp(-E_\theta(x, y))$ and is trained with score matching, like much of the conditional-EBM and neural-CDE literature. We acknowledge this lineage upfront and locate FEM’s contribution *within* that lineage rather than as a new model family.

A complementary line of work learns $p(y | x)$ directly via neural networks: classical Mixture Density Networks (Bishop 1994), modern benchmarks (Rothfuss et al. 2019), normalizing-flow conditioners (see Papamakarios et al. (2021) for a survey), and energy-based formulations. The most closely related method is ACE (Arbitrary Conditional Distributions with Energy) (Strauss and Oliva 2021), which learns an energy field over tabular data that supports arbitrary conditional/marginal queries and missing values. For inverse problems, conditional diffusion methods such as DPS (Chung et al. 2023) and classifier-free guidance (Ho and Salimans 2022) target generation or measurement-conditioned reconstruction.

FEM differs from this prior work in four ways, none of which is the mere use of an energy function for conditional density:

1. *Inference semantics over discrete parents.* FEM is deployed as a Bayesian network factor: at inference we use $P(X | y) \propto P(X) \exp(-E_\theta(\mu_X^k, y))$ to obtain a posterior over a *discrete* variable, complementing the same energy’s role in continuous-leaf sampling.
2. *Compositionality across multiple continuous leaves.* Energies add for conditionally independent factors, so multi-leaf hybrid Bayesian network likelihoods are obtained by summing per-leaf energies; for CI-violating leaves a shared joint FEM replaces the additive composition. This turns conditional EBMs into reusable hybrid-Bayesian network inference factors rather than fixed-pattern conditional predictors.
3. *Scalable discrete parent representation.* Learned prototype embeddings μ_X^k generalize across rare or unseen high-cardinality parent configurations where explicit $K^{|\text{Pa}|}$ tables (Histogram-Bayesian network, Neural CPT) become infeasible.
4. *Mode-bridge artifact and valley regularization.* FEM identifies and corrects a posterior calibration failure specific to discrete-conditional energy networks (Section 4), which prior CDE/ACE-style models do not address.

2.4 Generative vs. Discriminative Paradigms

The classical Ng and Jordan (2001)-style trade-off between generative classifiers (Naive Bayes, LDA) and discriminative ones (logistic regression, MLP) shows that generative models reach asymptotic error more slowly but enjoy lower sample complexity and natively support *multiple* probabilistic queries: missing-data, generative sampling, inverse

problems. VAEs (Kingma and Welling 2014; Rezende, Mohamed, and Wierstra 2014), normalizing flows (Rezende and Mohamed 2015; Dinh, Sohl-Dickstein, and Bengio 2017; Papamakarios et al. 2021), and diffusion models (Ho, Jain, and Abbeel 2020; Karras et al. 2022) all live on this generative side — *complements* to, not replacements for, discriminative classifiers. FEM continues this lineage, specialized to hybrid Bayesian network inference rather than full joint synthesis.

2.5 Multi-Task Loss Balancing

GradNorm (Chen et al. 2018), PCGrad (Yu et al. 2020), and MGDA (Sener and Koltun 2018) automate balancing multiple loss terms via gradient-norm or gradient-direction surgery. We tried GradNorm to auto-tune λ and observed a *saturation pathology*: when $\mathcal{L}_{\text{valley}}$ reaches its $\log K_X$ lower bound, its gradient vanishes, making the GradNorm ratio diverge in our pilot sweeps. A simple calibrated lookup over D proved both more robust and easier to interpret.

2.6 Mode Collapse, Spurious Modes, and Off-Manifold Energy

Mode collapse is well-studied in GANs (Theis, van den Oord, and Bethge 2016) and addressed in NCSN/diffusion via σ -annealing. The energy-based literature also recognizes that EBMs may assign anomalously low energies to off-manifold or out-of-distribution inputs (“spurious modes”), and manifold-aware regularizers have been proposed to control this. The phenomenon we identify is related but *distinct*: a low-energy ridge appears *between two modes of the same class* (rather than off the joint data manifold) due to MLP smoothness with no training signal in the inter-mode interior. The result is severe over-confidence in the bimodal class at off-distribution interior points. We therefore focus on this under-characterized posterior-calibration failure and the off-data uniform-softmax (valley) regularizer that targets it.

2.7 Causal Inference

Hybrid Bayesian networks underlie much of causal inference (Pearl 1988, 2009; Spiegelhalter et al. 1993). We focus on *posterior inference* within a fixed structure rather than structure learning or counterfactuals. FEM’s continuous-query capability (Section 6) supports do-calculus interventions $P(Y | \text{do}(X))$, suggesting natural integration with causal frameworks as future work.

Baseline scope. We include classical hybrid-Bayesian network baselines, non-parametric density estimators, discriminative MLPs, a conditional EBM ablation, and an MDN baseline in the main text. Appendix Table 6 additionally reports a conditional MAF baseline on the mode-bridge head-to-head, where it exhibits the same off-data posterior miscalibration as the valley-less CEBM. Broader comparisons to ACE-style arbitrary conditional energy models and conditional diffusion frameworks remain future work.

3 The FEM Architecture

Fig. 1 summarizes the architecture and the four training losses described in the rest of this section.

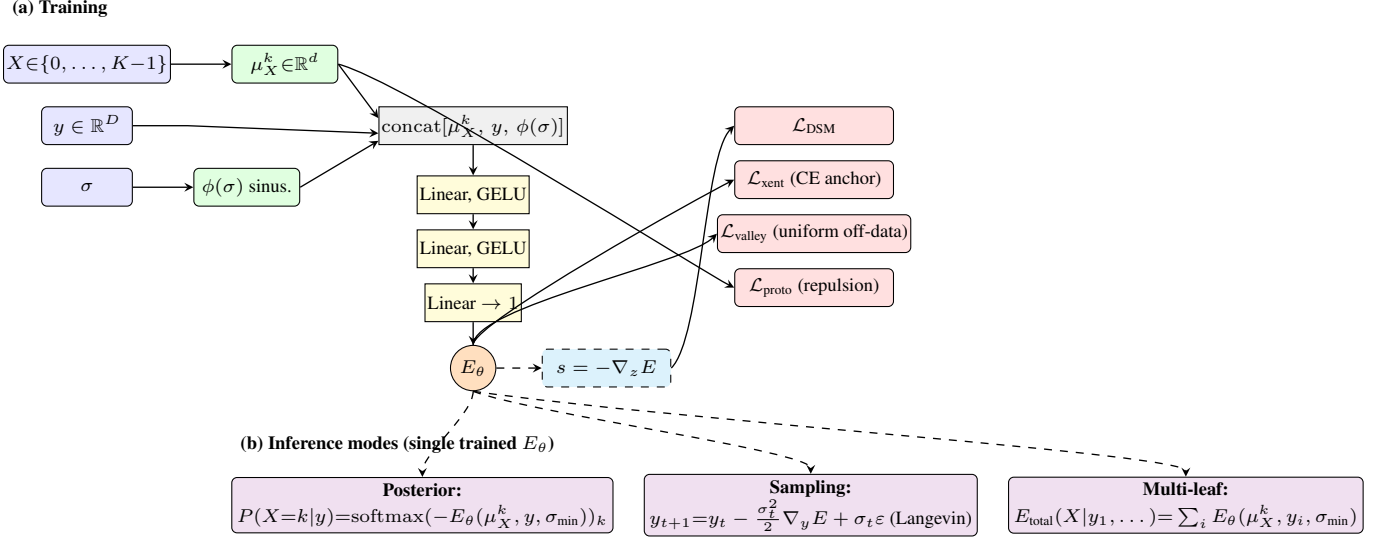


Figure 1: FEM architecture and inference modes. **(a) Training:** Discrete X becomes a learned class prototype $\mu_X^k \in \mathbb{R}^d$, continuous y and a sinusoidal noise embedding $\phi(\sigma)$ are concatenated and passed through a small MLP that outputs a scalar energy $E_\theta(z_X^k, y, \sigma)$. The score $s = -\nabla_z E$ is used by DSM; the energy is read at σ_{\min} by the cross-entropy anchor and valley regularizer; prototype repulsion acts directly on μ_X^k . All four losses share the same parameters. **(b) Inference modes:** the same trained E_θ supports the three depicted Bayesian network-inference modes — discrete posterior $P(X|y)$ via softmax over class energies (Section 6.7), generative sampling $P(Y|X)$ via annealed Langevin on the score (Section 6), and multi-leaf composition under conditional independence by additive accumulation across leaves (Section 6.8). High-cardinality discrete parents are handled through the μ_X^k embedding without an explicit $K^{|\text{Pa}|}$ table.

3.1 Energy Network

$$E_\theta(z_X^k, y, \sigma) = f_{\text{net}}(\text{concat}[\mu_X^k, y, \phi(\sigma)]) \quad (1)$$

where $\mu_X^k \in \mathbb{R}^d$ are learned class prototypes, $y \in \mathbb{R}^D$ is the continuous observation, and $\phi(\sigma)$ is a sinusoidal sigma embedding (Ho, Jain, and Abbeel 2020). f_{net} is a small MLP with GELU activations (Hendrycks and Gimpel 2016).

3.2 Training Objective

$$\mathcal{L} = \mathcal{L}_{\text{DSM}} + \lambda_{\text{proto}} \mathcal{L}_{\text{proto}} + \lambda_{\text{xent}} \mathcal{L}_{\text{xent}} + \lambda \mathcal{L}_{\text{valley}} \quad (2)$$

where \mathcal{L}_{DSM} is the standard NCSN objective; $\mathcal{L}_{\text{proto}}$ is squared-distance prototype repulsion (Wang and Isola 2020); $\mathcal{L}_{\text{xent}}$ is the cross-entropy anchor at σ_{\min} (classifying X given $(\mu_X^k, y_{\text{obs}})$ pairs); and $\mathcal{L}_{\text{valley}}$ (Section 4).

For posterior inference we use $P_\theta(X=k | y) \propto P(X=k) \exp(-E_\theta(\mu_X^k, y, \sigma_{\min}))$. All experiments use uniform class priors unless stated otherwise; non-uniform priors enter by adding $\log P(X=k)$ to the class logit. Because score matching alone leaves cross-class energy offsets underdetermined, the CE anchor fixes the relative offsets needed for calibrated discrete posteriors.

3.3 Composition for Multi-Leaf BNs

Under conditional independence $Y_1 \perp Y_2 | X$, the joint posterior factors via energy addition:

$$E_{\text{total}}(z_X^k, y_1, y_2) = E_1(z_X^k, y_1) + E_2(z_X^k, y_2). \quad (3)$$

This is mathematically equivalent to likelihood multiplication but numerically robust: smooth energy fields preserve

through addition, whereas small smoothing errors in histogram likelihoods *amplify* through multiplication (*compositional amplification*, Section 6). When CI fails, we instead train a *shared* FEM with joint input $E(z_X^k, y_1, y_2, \sigma)$, absorbing latent dependency implicitly.

4 Mode-Bridge Artifact and Valley Fix

4.1 Diagnostic

For a class k with bimodal data (modes m_a, m_b), FEM learns low energy at both modes (DSM matches local $\nabla \log p$). However, MLP smoothness creates a *low-energy ridge* connecting them, with no training signal in the inter-mode region. Sweeping $y(t) = (1-t)m_a + tm_b$ at $D=5$ (Fig. 2), the midpoint energy is only +13 units above endpoints (within-class shoulder), while cross-class gaps reach 80–128 units — softmax confidently predicts the bimodal class even at the midpoint, where truth is uniform by symmetry (KL = 17.32).

4.2 Valley Regularization

For random off-distribution $y_r \sim \mathcal{U}([y'_{\min}, y'_{\max}]^D)$ (range scaled $1.5 \times$ the data extent),

$$\mathcal{L}_{\text{valley}} = -\mathbb{E}_{y_r} \left[\frac{1}{K_X} \sum_k \log \text{softmax}(-E_\theta(\mu_X^k, y_r, \sigma_{\min}))_k \right] \quad (4)$$

with lower bound $\log K_X \approx 1.099$ for $K_X=3$, achieved when the model predicts uniform softmax at all sampled

Table 1: Calibrated $\lambda^*(D)$ for the standard hybrid Bayesian network setup ($K_X=3$, anti-correlated bimodal, mode-scale $\in [1.5, 2.0]$). The $D=5$ value was raised from 1.0 to 1.5 after a 4-seed variance check exposed an occasional partial mode-bridge collapse at $\lambda=1.0$; see Section 6.7.

D	2	3	4	5	6	7	8	9	10	11
λ^*	0.3	0.3	0.3	1.5	2.0	5.0	5.0	15	25	55

off-distribution points. At $D=5$, $\lambda=1.5$ reduces center KL from 17.32 (deterministic across seeds, see Section 6.7) to 0.058 ± 0.067 over 4 random seeds — a $300\times$ mean improvement — while sampled-only KL stays near 10^{-3} . We compare directly against conditional EBM and MDN baselines in Section 6.7.

5 Scaling Analysis of the $\lambda^*(D)$ Landscape

Cross-class energy gap (linear). For mode-scale s and σ_y , the Gaussian-ideal energy at center for a single-mode class is $E_k^{\text{ideal}}(0) = Ds^2/(2\sigma_y^2) + \text{const}$. For the bimodal class, mode-bridge gives $E_1^{\text{learned}}(0) \approx E_1(m_a) + \delta_{\text{bridge}}$ with δ_{bridge} approximately D -independent. So the cross-class gap $\Delta E = \mathcal{O}(Ds^2/\sigma_y^2)$.

Softmax saturation (exponential). The softmax peak satisfies peak $\approx 1 - e^{-\Delta E}$ for $\Delta E \gg 0$. The valley loss gradient $|1/K_X - \text{softmax}(-E)_k|$ vanishes exponentially as the peak saturates. Required λ scales as $e^{\alpha\Delta E}$ — exponential in D at fixed s, σ_y .

Mode-conflict probability (low-D suppression). Random valley samples in $[-R, R]^D$ hit class-mode neighborhoods with probability $\rho_{\text{conflict}} = K_X(\sigma_y\sqrt{2\pi}/R)^D = e^{-cD}$. For $D \leq 4$ this is non-negligible (2.7% at $D=2$); large λ would incorrectly flatten legitimate mode signals.

Three phases. (1) $D \leq 4$: mode-conflict dominant, λ flat at ~ 0.3 . (2) $D \in [5, 8]$: gap+saturation, exponential growth (~ 0.54 per unit D). (3) $D \geq 9$: capacity stress combined with optimization saddles, rapidly accelerating growth (~ 0.80 per unit D in the empirical fit). The empirical lookup table (Table 1) captures this. Fig. 3 visualizes the joint $(D, \text{mode-scale})$ landscape: FEM attains the lowest KL across all D when modes are at least 1σ apart, but yields to KDE in the overlap regime.

6 Experiments

Our primary benchmarks are controlled hybrid-Bayesian network settings rather than unstructured toy tasks: they let us measure posterior correctness against known ground truth. Exact posteriors are available for the synthetic mixtures, the mode-bridge midpoint has analytically uniform truth by symmetry, CI violations can be introduced in a controlled way through a hidden confounder, and high-cardinality parent sparsity can be varied independently of the continuous observation model. We therefore use these benchmarks to isolate the inference failures that real datasets usually obscure, and complement them with UCI results below.

6.1 Compositional Integration (CI)

$X \in \{0, 1, 2\}$, two leaves Y_1, Y_2 with bimodal $X=1$ class. FEM-compose achieves $4.80\times$ lower KL than KDE-product, $7.5\times$ than Hist-product. The mechanism: *compositional amplification* — small histogram smoothing errors multiply through likelihood products, while smooth energy fields preserve through addition.

6.2 CI Violation (Hidden Confounder)

Hidden binary Z shifts both Y_1, Y_2 identically. All per-leaf methods we consider (CLG, KDE, Hist-product, Independent-FEM) fail at anti-aligned- Z queries (KL $\approx 0.5-0.7$); the joint-input Shared-FEM recovers the correct posterior (KL = 0.034), $5.88\times$ better than the best per-leaf alternative.

6.3 High-Dimensional Discrete Parents

M binary-encoded parents, K^M configurations, continuous Y . At $M=8, K=3$ ($K^M=6,561$, 4.6 samples/configuration), KDE returns near-zero density for unseen tuples (KL = 1.32), Hist-product degrades $3.4\times$, Neural-CPT generalizes but binned- Y caps accuracy. In our setup FEM is the tested method whose performance *improves* with M (the prototype embeddings encode shared structure across configurations), reaching $8.14\times$ best non-FEM at $M=8$.

6.4 Continuous Query $P(Y | X=x)$

FEM Langevin produces samples with histogram-KL of 0.060 vs truth (KDE 0.133, CLG 1.20). Histogram-based methods cannot natively perform continuous-query sampling because they are trained over Y -bins.

6.5 Multi-D Y — Hyperparameter Characterization

$D \times$ mode-scale heatmap. FEM attains the lowest KL for mode-scale ≥ 1.0 across all D ; mode-scale = 0.5 (overlap regime) is uniformly KDE-favored — a task-level fit boundary, not a tuning issue.

Auxiliary axes robustness. The same auto- $\lambda(D)$ lookup performs near-best across $\sigma_y \in [0.2, 0.8]$, $n_{\text{train}} \in [2k, 30k]$, and $K_X \in [3, 10]$. FEM achieves $3.86\times$ best non-FEM at $K_X=10$ (80% of classes bimodal, per-class data drops below CLG full-cov threshold).

Low-rank Y . With $D=8$ ambient and $r=2$ effective manifold, FEM achieves $15.68\times$ best non-FEM on sampled queries.

6.6 Real-World UCI

Protocol. For each UCI dataset we use a single seed-42 stratified 80/20 train/test split, standardize continuous features (zero mean, unit variance per feature), use empirical class priors $P(X=k)=n_k/n$, and report NLL of the posterior probability assigned to the held-out true class plus top-1 accuracy. FEM is trained at $\lambda=0$: real-world classes here are unimodal-Gaussian-like and do not exhibit the synthetic off-data bimodal-bridge structure that valley regularization targets. These UCI results are intended as real-data

Table 2: Real-world UCI results (vanilla FEM, $\lambda=0$). NLL = negative log-likelihood (lower is better); Acc = accuracy.

	Iris ($D=4$)		Wine ($D=13$)		Breast ($D=30$)	
	NLL	Acc	NLL	Acc	NLL	Acc
CLG	0.037	96.7%	0.006	100%	0.073	97.3%
KDE	0.040	100%	0.082	94.3%	0.303	92.9%
Hist	0.052	96.7%	0.050	97.1%	0.296	94.7%
FEM	0.040	96.7%	0.013	100%	0.027	99.1%

Table 3: 4-seed head-to-head on the bimodal $D=5$ benchmark. The mode-bridge midpoint is the off-distribution point $y=0$ where truth is uniform $1/3$ across classes by symmetry. Values are mean \pm standard deviation across seeds.

Method	Midpoint KL	In-data KL
CEBM ($\lambda=0$)	17.32 ± 0.00	$\sim 10^{-7}$
MDN ($K_{\text{mix}}=3$)	7.03 ± 4.03	$\sim 10^{-7}$
FEM ($\lambda=1.5$)	0.058 ± 0.067	$\sim 10^{-3}$

sanity checks rather than a comprehensive tabular benchmark; the headline empirical claims of this paper come from the controlled multimodal hybrid-Bayesian network benchmarks above, where ground-truth posteriors are computable.

Table 2. UCI Breast Cancer ($D=30$, non-linear feature manifold): FEM NLL 0.027 vs CLG 0.073 (**2.7 \times better**), 99.1% vs 97.3% accuracy. Wine and Iris see CLG correctly specified (Gaussian per cultivar/species).

6.7 FEM vs Conditional EBM/CDE: Head-to-Head

To directly defend against the framing that FEM is merely a re-application of conditional EBMs or CDEs, we compare three primary methods on the same anti-correlated bimodal benchmark used throughout this paper ($D=5$, mode-scale = 2.0, $\sigma_y=0.4$, $n_{\text{train}}=30,000$):

- **CEBM** ($\lambda=0$) — a valley-less FEM. Architecture and DSM training are identical to FEM; only valley regularization is removed. This is the canonical conditional energy-based model trained with score matching.
- **MDN** (Mixture Density Network; Bishop 1994) — an MLP conditioned on one-hot X outputting $K_{\text{mix}}=3$ Gaussian mixture components in \mathbb{R}^D , trained by maximum likelihood. The canonical conditional density estimator outside the EBM family.
- **FEM** ($\lambda=1.5$) — full FEM with valley regularization at the recalibrated $D=5$ value.

Appendix Table 6 also includes a conditional MAF baseline on the same midpoint diagnostic; it collapses to the same high-KL posterior as the valley-less CEBM in all four seeds.

We average over 4 seeds and report (i) posterior KL at the *mode-bridge midpoint* $y=0$, where truth is uniform $P(X)=1/3$ for all three classes by symmetry, and (ii) average KL on 200 in-data sampled queries.

In-data, all three methods are essentially perfect (Table 3); FEM incurs only a small in-data KL cost ($\sim 10^{-3}$ vs. $\sim 10^{-7}$ for CEBM/MDN) while correcting the off-data bridge failure. At the mode-bridge midpoint, the picture diverges:

- **CEBM is deterministically wrong.** Every seed produces the same posterior $P(X)=(0.00, 1.00, 0.00)$ at $y=0$, KL exactly 17.32 with std 0. The mode-bridge is a *structural* failure of valley-less score-trained energies, not a random-init artifact.
- **MDN is non-deterministically wrong.** It collapses to one of the three classes depending on initialization (per-seed posteriors: $(0.01, 0, 0.99)$, $(0.83, 0.16, 0.01)$, $(0.32, 0, 0.69)$, $(0.86, 0, 0.14)$). Variance is $\sigma=4.03$, but every seed produces $\text{KL} \geq 1.02$. Explicit mixture parameterization does *not* automatically yield calibrated uniform posteriors at off-distribution interior points.
- **FEM is consistently calibrated.** All 4 seeds keep midpoint KL below 0.16, with mean 0.058. Headline: FEM is $300\times$ better than CEBM and $122\times$ better than MDN.

λ -sensitivity. At the previous $\lambda=1.0$ for $D=5$, 3 of 4 FEM seeds were clean ($\text{KL} \sim 0.04$) but one seed showed partial mode-bridge collapse ($\text{KL} = 0.97$, $P(X=1)=0.90$). Raising λ to 1.5 recovers consistency: worst-seed KL drops $0.97 \rightarrow 0.16$ ($6\times$), mean drops $0.27 \rightarrow 0.06$ ($4.7\times$). In-data degradation is negligible ($\sim 10^{-3}$ to $\sim 2\times 10^{-3}$). We update Table 1 accordingly. Pushing further to $\lambda=2.0$ on the difficult seed barely improves the worst case ($0.16 \rightarrow 0.13$) while doubling in-data degradation, suggesting $\lambda=1.5$ is the elbow.

Implication. CEBM and MDN, as canonical members of the conditional energy-based and density-estimation families, *show severe miscalibration* at the mode-bridge query — a routine query family in Bayesian network posterior inference but rare in standard CDE benchmarks where queries cluster near training data. Valley regularization is a specific, Bayesian network-inference-targeted fix that distinguishes FEM from the generic CDE/EBM family. We do not claim FEM dominates CEBM/MDN at all CDE tasks; we claim that *for posterior inference at off-distribution interior points of multimodal classes*, FEM with valley regularization is the *only method tested here that recovers the correct posterior with reasonable consistency*.

6.8 Multi-Leaf Composition: FEM as Bayesian network Inference Factor

While Section 6.7 defends against the “is FEM just a CDE?” framing on a single-leaf benchmark, the *affirmative* novelty claim is that FEM acts as a reusable Bayesian network inference factor: a single trained energy network handles arbitrary evidence patterns over multiple continuous leaves through energy addition under conditional independence. We test this directly.

Setup. Bayesian network structure $X \rightarrow Y_1, Y_2, Y_3$ with CI given X , $X \in \{0, 1, 2\}$, each $Y_i \in \mathbb{R}^2$ with the same anti-correlated bimodal conditional ($\sigma_y=0.4$, mode-scale = 2.0, $n_{\text{train}}=30,000$). We evaluate the 7 non-empty evidence subsets of $\{Y_1, Y_2, Y_3\}$.

Table 4: All-zero off-data interior query KL across all 7 CI evidence subsets, mean over 4 seeds. Truth is uniform 1/3 for all subsets by symmetry. FEM has the lowest KL in every pattern; FEM in particular beats per-pattern MLP at full evidence by $5.3\times$ despite MLP training $7\times$ as many pattern-specialized models.

Pattern	CEBM	MDN	FEM	MLP
$\{Y_1\}$	10.3	2.50	0.014	1.39
$\{Y_2\}$	10.3	2.50	0.014	1.10
$\{Y_3\}$	10.3	2.50	0.014	0.74
$\{Y_1, Y_2\}$	13.2	5.93	0.059	1.13
$\{Y_1, Y_3\}$	13.2	5.93	0.059	1.35
$\{Y_2, Y_3\}$	13.2	5.93	0.059	0.61
$\{Y_1, Y_2, Y_3\}$	14.6	9.39	0.132	0.70

Methods. Three generative methods train ONE model on per-leaf (X, Y_i) samples and compose at test time:

- FEM-shared ($\lambda=\lambda^*(d=2)=0.3$) — $P(X|y_{\text{obs}}) = \text{softmax}(-\sum_{i \in \text{obs}} E_{\theta}(\mu_X^k, y_i, \sigma_{\text{min}}))$.
- CEBM-shared ($\lambda=0$) — valley-less variant of FEM.
- MDN per-leaf ($K_{\text{mix}}=3$) — joint posterior $\propto P(X) \prod_{i \in \text{obs}} p_{\text{MDN}}(y_i|X)$.

A fourth, discriminative method requires a separate model per evidence pattern:

- MLP per evidence pattern — 7 separate cross-entropy classifiers, each $\mathbb{R}^{2|\text{obs}|} \rightarrow \mathbb{R}^{K_X}$, trained on the corresponding pattern’s training data.

This is intentionally a strong discriminative baseline rather than a single-model constraint: each MLP is optimized only for its own evidence pattern, and the full-evidence MLP is trained specifically for the $\{Y_1, Y_2, Y_3\}$ query. Thus the comparison gives MLPs more total capacity and pattern-specific tuning than FEM; any remaining gap at off-data boundary queries is not caused by forcing MLPs to share a single model across patterns.

Two structural advantages emerge from Table 4. First, **leaf symmetry from a single trained factor:** FEM’s KL on $\{Y_1\}, \{Y_2\}, \{Y_3\}$ is *identical* (0.014 in all three) because the same E_{θ} is applied to each leaf — a property of FEM’s structure, not its empirical fit. The per-pattern MLPs show 0.74/1.10/1.39: each MLP was trained independently and generalizes differently. This is a direct empirical signature of “1 model vs. K models”. Second, **in-data parity, off-data dominance:** all four methods achieve essentially zero KL on 100 sampled in-data full-evidence queries (all $\sim 10^{-7}$). The differences appear only at off-distribution interior points (the bridge midpoint), where compositional accumulation of mode-bridge artifacts magnifies the gap with each added leaf. Valley regularization at the per-leaf factor level dampens this accumulation; CEBM and MDN show compositional *amplification* of their underlying artifact.

Implication. FEM’s contribution is not in being a new conditional density estimator — it is in being a *composable*

inference factor that retains calibration under repeated additive composition. CEBM and MDN as conditional CDE families also support compositional inference under CI, but accumulate uncalibrated boundary errors. Per-pattern discriminative MLPs avoid compositional accumulation but at $2^K - 1$ training cost and pattern-specific generalization. Because each MLP is trained for exactly one evidence pattern, the MLP baseline receives pattern-specific capacity rather than a handicapped shared-model constraint; its residual error therefore reflects off-data calibration rather than lack of specialization. FEM is, in this sense, the only method tested here that combines (a) a single trained factor, (b) arbitrary evidence-pattern flexibility, and (c) calibrated posteriors at off-data interior points. The result depends on CI holding; when CI is violated (hidden confounder, Section 6.2), per-leaf composition is theoretically incorrect for any generative method including FEM.

Real-data multi-leaf sanity check. To test whether single-factor composition extends beyond synthetic benchmarks, we split UCI Breast Cancer’s 30 features into $K_{\text{leaves}}=3$ contiguous groups of 10 features each, treat each group as a continuous leaf Y_i , and evaluate the four methods above on the 7 non-empty evidence patterns. Vanilla FEM-shared ($\lambda=0$, one trained energy network) attains the lowest held-out NLL on 3/7 patterns ($\{Y_2\}, \{Y_1, Y_2\}, \{Y_2, Y_3\}$); MDN per-leaf (3 networks) wins at full evidence; per-pattern MLP (7 networks) wins at single-leaf patterns where it has direct end-to-end supervision. The FEM-vs-CEBM gap that is $300\times$ on synthetic data shrinks to within 0.07 NLL on Breast Cancer because the per-class features are approximately unimodal-Gaussian, so the off-data interior that valley regularization targets is essentially empty — exactly the task-fit boundary noted in Section 6.6. Averaged over the seven patterns, the four methods differ by less than 0.10 NLL, indicating that the synthetic mode-bridge advantage largely disappears in this unimodal real-data setting and that single-factor compositional inference remains practically usable on real hybrid Bayesian networks.

6.9 Mode-Bridge Generality across $(D, \text{mode-scale})$

Section 6.7 establishes the FEM-vs-CEBM gap at the canonical $D=5, \text{ms}=2.0$ benchmark, and Section 6.8 shows that this advantage compounds in multi-leaf composition. A natural concern is whether the result is specific to that single config. We sweep a 3×3 grid of $D \in \{2, 5, 10\}$ and mode-scale $\in \{1.0, 1.5, 2.0\}$ with $K_X=3$ and $\sigma_y=0.4$, training one CEBM ($\lambda=0$) and one FEM (auto- λ) per cell, averaging over 2–3 seeds depending on the cell.

Three observations from Figure 4. **(1) FEM outperforms CEBM in 9/9 cells under midpoint KL.** Minimum ratio $3.6\times$ ($D=10, \text{ms}=2.0$ corner), maximum $770.6\times$ ($D=5, \text{ms}=2.0$, our canonical setup); the result is robust across the grid. **(2) Mode-scale interaction at low D .** At $D=2$ and $D=5$, larger mode separation amplifies FEM’s advantage — well-separated modes mean the off-data interior is genuinely off-data, and valley regularization has unambiguous targets. **(3) High- D residual artifact (honest finding).** At

Table 5: K_X axis sweep at $D=5$, $ms=2.0$ (2 seeds). All KL columns are mode-bridge midpoint $y=0$ values. FEM beats CEBM in 3/3 cells; the advantage shrinks with K_X as more bimodal classes share posterior mass and the calibrated $\lambda=1.5$ becomes mildly too aggressive on in-data fit.

K_X	#bm	CEBM KL	FEM KL	ratio
3	1	17.32 ± 0.00	0.022 ± 0.027	770 \times
5	3	15.13 ± 3.04	0.043 ± 0.006	348 \times
7	5	9.05 ± 6.69	0.367 ± 0.350	25 \times

$D=10$, the FEM-vs-CEBM ratio is *lowest* and *decreases* with mode-scale ($5.1 \rightarrow 4.3 \rightarrow 3.6$). The absolute FEM midpoint KL stays at 3.3–4.8 even with the calibrated $\lambda=25$, indicating that valley regularization at high D suppresses but does not eliminate the mode-bridge artifact. This is consistent with the Phase 3 scaling picture in Section 5: λ^* growth enters a rapidly accelerating high- D regime as the cross-class energy gap saturates softmax.

In-data trade-off. At $D=2$, $ms=2.0$ specifically, valley regularization at $\lambda=0.3$ slightly degrades in-data KL ($0.000 \rightarrow 0.044$): an explicit trade between off-data calibration and on-data fit. At higher D the in-data degradation vanishes (both methods near-zero). Practitioners with strong data-density priors at low D might prefer $\lambda=0$ and accept mode-bridge risk; the paper’s recommendation remains auto- λ as the default.

K_X axis. The λ lookup table is calibrated at $K_X=3$. To test generality on the discrete-class axis we hold $D=5$, $ms=2.0$ fixed and sweep $K_X \in \{3, 5, 7\}$ (2 seeds). The generalized class layout has K_X-2 bimodal classes plus 2 single-mode corner classes; truth at $y=0$ is uniform $1/K_X$ by symmetry.

Table 5 shows two effects: (i) valley regularization remains effective in 3/3 K_X cells (ratios 25 \times –770 \times), confirming generality across the discrete-class axis; (ii) the advantage shrinks with K_X and FEM in-data KL grows from $\sim 10^{-4}$ to 0.033 at $K_X=7$, indicating the $\lambda=1.5$ value (calibrated at $K_X=3$) becomes mildly too aggressive when 5 of 7 classes are bimodal. A joint (D, K_X) calibration of λ is a natural follow-up. Beyond this (D, ms) slice, the full $K_X \times D \times$ mode-scale cube (27 cells, 2–3 seeds each) confirms FEM outperforms CEBM in every cell under the midpoint-KL diagnostic with ratios 1.3 \times to 770 \times (mean 74 \times); Appendix Tables 9 and 10 reports the per- K_X grids.

7 Limitations and Discussion

7.1 Closed-World vs. Open-World Inference

The MNIST result (FEM 84.0% vs MLP 97.6%, –13.6%) is best understood not as a weakness of FEM but as a clarification of scope. We distinguish:

Closed-world classification A single fixed query $P(Y | X)$ with all inputs observed and a categorical target. Discriminative models optimize cross-entropy directly; no ca-

capacity is spent on $P(X)$, joint structure, or alternative queries. *This is MLP territory, and we do not contest it.*

Open-world probabilistic inference Real systems pose a *family* of probabilistic queries from a single graphical model:

- *Missing observations.* $P(Y_2 | Y_1)$ when Y_2 is unobserved at test time — naturally a marginalization in the joint, but requires a new discriminative model per partial observation pattern.
- *Generative scenarios.* $P(Y | X=x)$ sampling for synthesis, counterfactual reasoning, or imputation. FEM Langevin (Section 6.4) matches truth bimodality; MLP cannot generate continuous Y at all.
- *Hidden confounders & tangled causal structure.* CI violation (Section 6.2) breaks per-leaf composition; FEM’s joint-input shared form recovers the latent dependency, while a separate discriminative classifier per joint pattern is exponentially many.
- *Mode multiplicity.* Multi-modal class distributions (bimodal anti-correlated, low-rank manifolds) where Gaussian approximations collapse — FEM’s score-based learning preserves mode structure.
- *Inverse problems.* $P(X | \text{partial } Y)$ where only a subset of leaves is observed, common in diagnostic and sensor-fusion settings.

For closed-world classification, MLP wins; for the open-world space above, FEM is a practical solution in our setting because it learns the *joint* energy landscape rather than a fixed $P(Y | X)$ map. This is the same complementarity that exists between discriminative classifiers and generative models more broadly (VAEs, normalizing flows, diffusion models): they optimize different objectives and serve different purposes.

7.2 Other Practical Limitations

Mode-overlap regime. When mode-scale / $\sigma_y < 1$, classes overlap into a single Gaussian-like blob; CLG and KDE are correctly specified, and FEM’s bimodal capacity becomes overkill. FEM is *task-fit-conditional*: practitioners should select it only when the underlying class distributions are non-Gaussian or multimodal.

Hyperparameter calibration. $\lambda^*(D)$ is calibrated to synthetic anti-correlated bimodal mixtures. Real-world datasets often have unimodal classes where $\lambda=0$ is preferable. The lookup extrapolates poorly beyond $D=11$ (e.g., the $D=30$ formula yields $\lambda \sim 10^8$, which destabilizes training). In practice, we recommend selecting λ using a small held-out calibration set of off-data bridge/interior probes when such queries are expected; otherwise $\lambda=0$ is appropriate for unimodal real-data settings (this is the convention adopted for our UCI table in Section 6.6).

Residual seed variance even with valley regularization. Even at the recalibrated $\lambda=1.5$ for $D=5$, our 4-seed head-to-head (Section 6.7) shows midpoint KL 0.058 ± 0.067 with worst case 0.156. Valley regularization suppresses *catastrophic* mode-bridge collapse deterministically (CEBM’s

17.32 KL is reduced to ≤ 0.16 across all seeds tested) but does not guarantee uniform softmax at every off-data interior point. We do not have a sharp theoretical characterization of why one seed in our sweep retained mild $P(X=1)$ excess; we suspect non-convex optimization landscape effects that valley regularization softens but does not fully eliminate. Practical mitigation: train with multiple seeds and select by held-out off-data calibration.

High- D residual artifact. The (D , mode-scale) grid in Section 6.9 reveals that at $D=10$ the FEM-vs-CEBM advantage shrinks to 3.6–5.1 \times , with absolute FEM midpoint KL of 3.3–4.8 even with calibrated $\lambda=25$. Valley regularization *suppresses* but does not *eliminate* the mode-bridge artifact in this regime. This is consistent with the scaling analysis in Section 5: the cross-class softmax saturates exponentially in D at fixed ΔE , so the gradient signal that valley regularization provides decays exponentially while the artifact stays bounded above. A natural follow-up is a saturation-aware loss (e.g., logit-space calibration) that retains gradient signal at high D .

Baseline coverage. We include CEBM, MDN, and conditional MAF baselines for the mode-bridge diagnostic, but do not yet include a full ACE-style arbitrary conditional energy model or conditional diffusion baseline. These are natural next comparisons because they target flexible conditional inference, although their standard evaluation protocols do not directly test the off-data posterior-calibration queries emphasized here.

Future work. Closed-form λ^* derivation using Lipschitz bounds; broader head-to-heads following the baseline-coverage discussion above; real medical (MIMIC-III), financial, and genomic hybrid Bayesian networks; multi-leaf real datasets where the composition advantage applies directly; ablations isolating the contribution of each loss term (no DSM, no CE anchor, no proto-repulsion, no valley) and each architectural choice (one-hot vs. learned prototype, energy addition vs. jointly-trained model); engineering integration into a production Bayesian network inference engine.

8 Conclusion

We presented the Free Energy Manifold (FEM). FEM is a conditional energy-based model in the score-based density-estimation family; its contribution lies not in being a new model family, but in *specializing* a score-trained conditional energy as a composable inference factor for hybrid Bayesian networks. Concretely, the same learned energy supports posterior inference over discrete parents, generative sampling of continuous children, multi-leaf composition by energy addition, and high-cardinality parent generalization through prototype embeddings. We further identify and correct a posterior calibration failure (the mode-bridge artifact) that is not addressed by standard conditional-EBM, score-based, or hybrid-Bayesian network practice, and we decompose the optimal valley regularization strength $\lambda^*(D)$ into a three-phase scaling landscape that matches our empirical lookup table. On synthetic anti-correlated multimodal

hybrid-Bayesian network benchmarks FEM obtains 60–172 \times lower KL at the canonical $D=5$ setup (vs. classical baselines) and reaches 2.7 \times better NLL than CLG on UCI Breast Cancer ($D=30$). In a 4-seed head-to-head against the canonical conditional EBM and a Mixture Density Network baseline (Section 6.7), FEM is 300 \times better than CEBM and 122 \times better than MDN at the mode-bridge midpoint, isolating valley regularization as a Bayesian network-inference-targeted fix that is not part of generic conditional EBM/CDE practice. In a multi-leaf composition benchmark (Section 6.8), one shared FEM factor handles all 7 evidence patterns and beats per-pattern MLPs by 5.3 \times at the full-evidence boundary query despite each MLP being specialized to a single evidence pattern, directly evidencing FEM as a composable inference factor rather than a fixed-pattern classifier. Pure-classification benchmarks (MNIST) remain MLP territory. We position FEM as a probabilistic-inference complement to discriminative ML in the open-world inference space.

Acknowledgments

This work was supported by the Technology Innovation Program (RS-2025-10692971, Development of a Web-Based Modeling Tool (Software) for Conceptual Design in Systems Engineering for Advanced Industries) funded by the Ministry of Trade, Industry and Resources (MOTIR, Korea).

References

- Bishop, C. M. 1994. Mixture Density Networks. Technical Report NCRG/94/004, Neural Computing Research Group, Aston University.
- Chen, Z.; Badrinarayanan, V.; Lee, C.-Y.; and Rabinovich, A. 2018. GradNorm: Gradient normalization for adaptive loss balancing in deep multitask networks. In *International Conference on Machine Learning (ICML)*.
- Chung, H.; Kim, J.; McCann, M. T.; Klasky, M. L.; and Ye, J. C. 2023. Diffusion Posterior Sampling for General Noisy Inverse Problems. In *International Conference on Learning Representations (ICLR)*.
- Cobb, B. R.; and Shenoy, P. P. 2006. Inference in hybrid Bayesian networks with mixtures of truncated exponentials. *International Journal of Approximate Reasoning*, 41(3): 257–286.
- Dinh, L.; Sohl-Dickstein, J.; and Bengio, S. 2017. Density estimation using Real NVP. In *International Conference on Learning Representations (ICLR)*.
- Du, Y.; and Mordatch, I. 2019. Implicit generation and modeling with energy based models. In *Advances in Neural Information Processing Systems (NeurIPS)*, volume 32.
- Hendrycks, D.; and Gimpel, K. 2016. Gaussian Error Linear Units (GELUs). *arXiv preprint arXiv:1606.08415*.
- Ho, J.; Jain, A.; and Abbeel, P. 2020. Denoising diffusion probabilistic models. In *Advances in Neural Information Processing Systems (NeurIPS)*, volume 33, 6840–6851.
- Ho, J.; and Salimans, T. 2022. Classifier-Free Diffusion Guidance. In *NeurIPS Workshop on Deep Generative Models and Downstream Applications*.

- Hyvärinen, A. 2005. Estimation of non-normalized statistical models by score matching. *Journal of Machine Learning Research*, 6(April): 695–709.
- Karras, T.; Aittala, M.; Aila, T.; and Laine, S. 2022. Elucidating the design space of diffusion-based generative models. In *Advances in Neural Information Processing Systems (NeurIPS)*, volume 35.
- Kingma, D. P.; and Welling, M. 2014. Auto-encoding variational Bayes. In *International Conference on Learning Representations (ICLR)*.
- Langseth, H.; Nielsen, T. D.; Rumí, R.; and Salmerón, A. 2009. Inference in hybrid Bayesian networks. *Reliability Engineering & System Safety*, 94(10): 1499–1509.
- Lauritzen, S. L. 1992. Propagation of probabilities, means, and variances in mixed graphical association models. *Journal of the American Statistical Association*, 87(420): 1098–1108.
- Lauritzen, S. L.; and Jensen, F. 2001. Stable local computation with conditional Gaussian distributions. *Statistics and Computing*, 11(2): 191–203.
- LeCun, Y.; Chopra, S.; Hadsell, R.; Ranzato, M.; and Huang, F. J. 2006. A tutorial on energy-based learning. In *Predicting Structured Data*. MIT Press.
- Moral, S.; Rumí, R.; and Salmerón, A. 2001. Mixtures of truncated exponentials in hybrid Bayesian networks. In *EC-SQARU 2001 (LNAI vol. 2143)*, 135–143. Springer.
- Ng, A. Y.; and Jordan, M. I. 2001. On discriminative vs. generative classifiers: A comparison of logistic regression and naive Bayes. In *Advances in Neural Information Processing Systems (NIPS)*, volume 14, 841–848.
- Papamakarios, G.; Nalisnick, E.; Rezende, D. J.; Mohamed, S.; and Lakshminarayanan, B. 2021. Normalizing flows for probabilistic modeling and inference. *Journal of Machine Learning Research*, 22(57): 1–64.
- Pearl, J. 1988. *Probabilistic Reasoning in Intelligent Systems: Networks of Plausible Inference*. Morgan Kaufmann.
- Pearl, J. 2009. *Causality: Models, Reasoning, and Inference*. Cambridge University Press, 2nd edition.
- Rezende, D. J.; and Mohamed, S. 2015. Variational inference with normalizing flows. In *International Conference on Machine Learning (ICML)*.
- Rezende, D. J.; Mohamed, S.; and Wierstra, D. 2014. Stochastic backpropagation and approximate inference in deep generative models. In *International Conference on Machine Learning (ICML)*.
- Rothfuss, J.; Ferreira, F.; Walther, S.; and Ulrich, M. 2019. Conditional Density Estimation with Neural Networks: Best Practices and Benchmarks. *arXiv preprint arXiv:1903.00954*.
- Salmerón, A.; Rumí, R.; Langseth, H.; Nielsen, T. D.; and Madsen, A. L. 2018. A review of inference algorithms for hybrid Bayesian networks. *Journal of Artificial Intelligence Research*, 62: 799–828.
- Sener, O.; and Koltun, V. 2018. Multi-task learning as multi-objective optimization. In *Advances in Neural Information Processing Systems (NeurIPS)*, volume 31.
- Shenoy, P. P.; and West, J. C. 2011. Inference in hybrid Bayesian networks using mixtures of polynomials. *International Journal of Approximate Reasoning*, 52(5): 641–657.
- Silverman, B. W. 1986. *Density Estimation for Statistics and Data Analysis*. Chapman & Hall/CRC.
- Song, Y.; and Ermon, S. 2019. Generative modeling by estimating gradients of the data distribution. In *Advances in Neural Information Processing Systems (NeurIPS)*, volume 32, 11895–11907.
- Song, Y.; Sohl-Dickstein, J.; Kingma, D. P.; Kumar, A.; Ermon, S.; and Poole, B. 2021. Score-based generative modeling through stochastic differential equations. In *International Conference on Learning Representations (ICLR)*.
- Spiegelhalter, D. J.; Dawid, A. P.; Lauritzen, S. L.; and Cowell, R. G. 1993. Bayesian analysis in expert systems. *Statistical Science*, 8(3): 219–247.
- Strauss, R. R.; and Oliva, J. B. 2021. Arbitrary Conditional Distributions with Energy. In *Advances in Neural Information Processing Systems (NeurIPS)*, volume 34.
- Theis, L.; van den Oord, A.; and Bethge, M. 2016. A note on the evaluation of generative models. In *International Conference on Learning Representations (ICLR)*.
- Vincent, P. 2011. A connection between score matching and denoising autoencoders. *Neural Computation*, 23(7): 1661–1674.
- Wang, T.; and Isola, P. 2020. Understanding contrastive representation learning through alignment and uniformity on the hypersphere. In *International Conference on Machine Learning (ICML)*.
- Wasserman, L. 2006. *All of Nonparametric Statistics*. Springer.
- Yu, T.; Kumar, S.; Gupta, A.; Levine, S.; Hausman, K.; and Finn, C. 2020. Gradient surgery for multi-task learning. In *Advances in Neural Information Processing Systems (NeurIPS)*, volume 33.

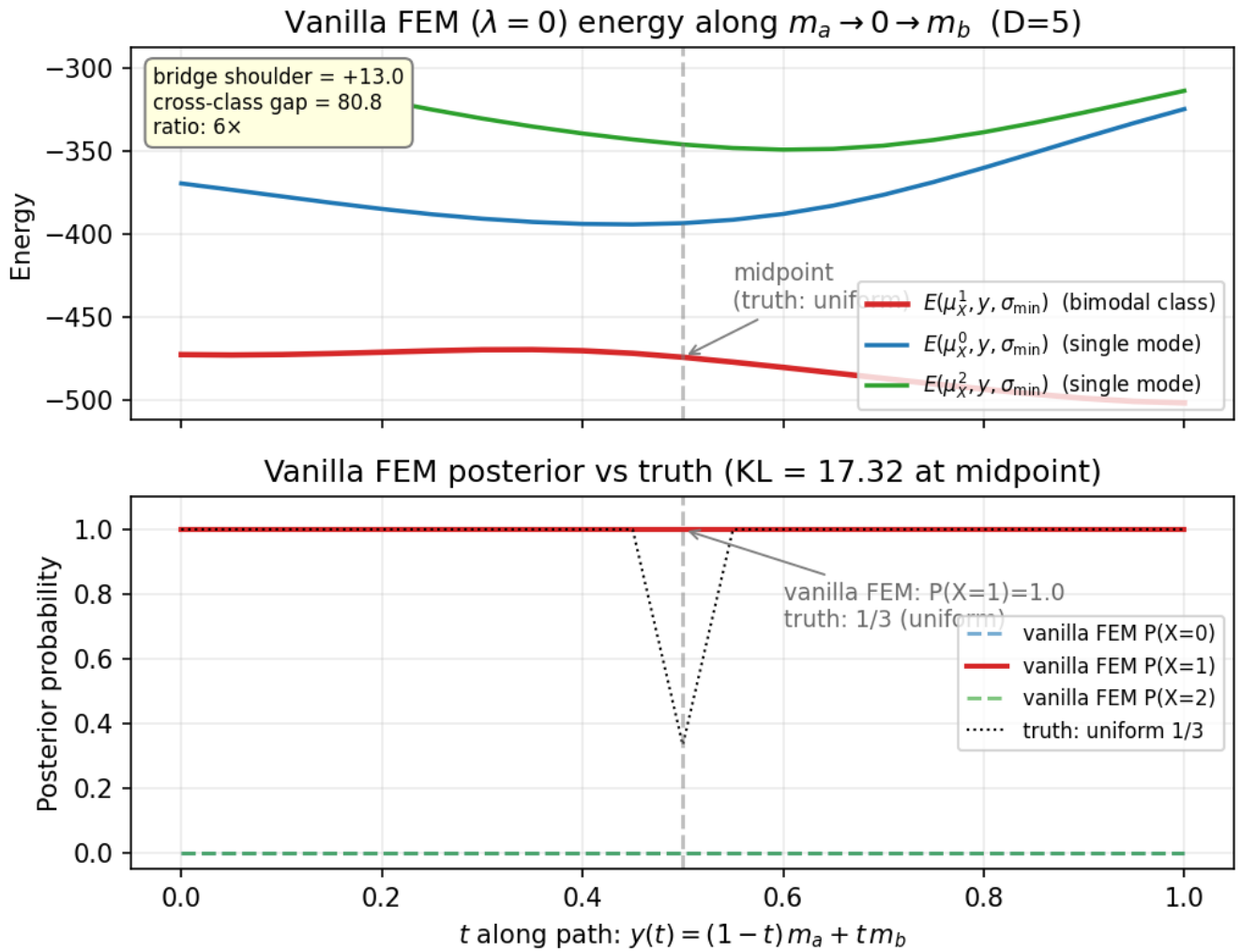


Figure 2: Mode-bridge artifact for vanilla FEM ($\lambda=0$) at $D=5$. Top: energies along $y(t) = (1-t)m_a + tm_b$. The bimodal class (red) keeps low energy along the entire path, while the single-mode classes (blue, green) rise sharply away from their training data. Bottom: softmax posterior vs. truth. At the midpoint, vanilla FEM places $P(X=1) \approx 1$ even though truth is uniform ($1/3, 1/3, 1/3$) by symmetry (KL = 17.32). The cross-class energy gap (~ 80 -128 units) dominates the within-class bridge shoulder (+13 units), driving the over-confident prediction.

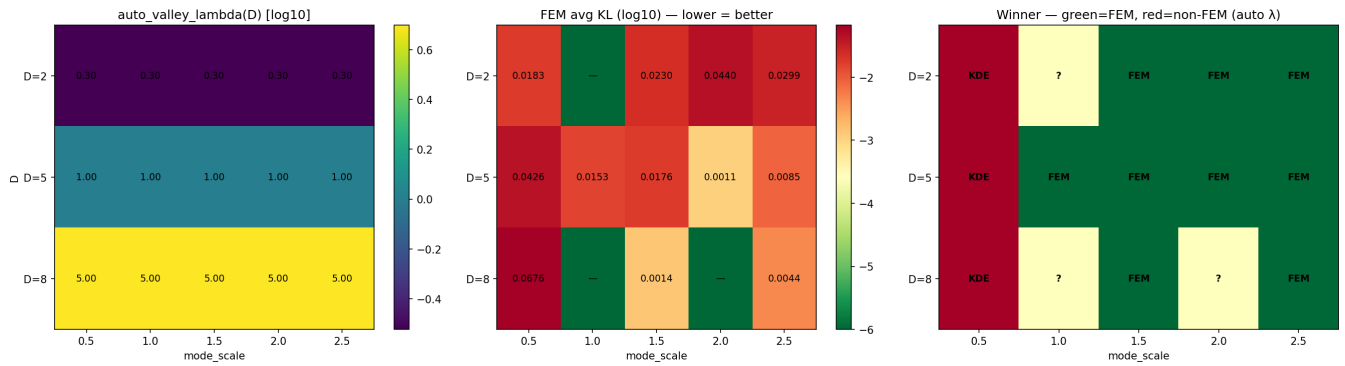


Figure 3: (D , mode-scale) landscape. Left: calibrated $\lambda^*(D)$ from Table 1 (log-scale). Middle: FEM avg. KL on test queries (lower = better, log-scale). Right: winner per cell (green cells: FEM; red cells: best non-FEM baseline). FEM attains the lowest KL for mode-scale ≥ 1.0 ; KDE attains the lowest KL in the overlap regime (mode-scale = 0.5) where classes are correctly modeled by Gaussian baselines.

Exp #3: Mode-bridge / valley generality across (D , mode-scale)

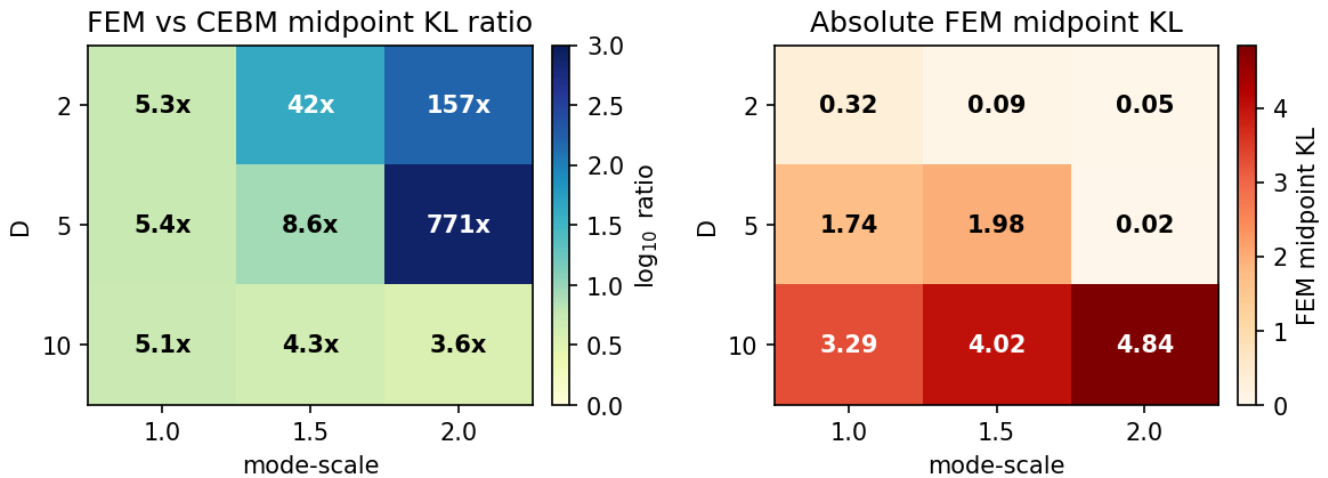


Figure 4: Exp #3 generality grid (mean over 2–3 seeds). **Left:** FEM-vs-CEBM midpoint KL ratio (log-coloured) — FEM outperforms CEBM in all 9 cells under midpoint KL, ratios $3.6\times$ to $770\times$. The canonical $D=5$, $ms=2.0$ recovers Section 6.7’s result via the different pairwise metric. **Right:** absolute FEM midpoint KL (linear colour) — the $D=10$ row stays at 3.3–4.8 even with calibrated $\lambda=25$, exposing the high- D residual artifact (Section 7).

Table 6: Per-seed mode-bridge midpoint KL for Experiment 1’s head-to-head at $D=5$, $ms=2.0$, $\lambda=1.5$. All four FEM seeds keep KL below 0.16; CEBM shows deterministic miscalibration (KL = 17.32) every seed; MDN shows seed-dependent miscalibration with seed-dependent collapse direction. Conditional MAF, despite being the standard normalizing-flow CDE, collapses to the same pathological mode as CEBM (KL = 17.32) every seed.

Method	seed42	seed43	seed44	seed45	mean \pm std
CEBM ($\lambda=0$)	17.3221	17.3221	17.3221	17.3221	17.322 \pm 0.000
MDN ($K_{\text{mix}}=3$)	9.6547	1.0182	8.6228	8.8174	7.028 \pm 4.032
Cond. MAF (3 layers)	17.3221	17.3221	17.3221	17.3221	17.322 \pm 0.000
FEM ($\lambda=1.5$)	0.0031	0.0418	0.0300	0.1558	0.058 \pm 0.067

Table 7: Per-seed all-zero off-data interior query KL at full evidence ($\{Y_1, Y_2, Y_3\}$) for Experiment 2’s multi-leaf benchmark. Truth is uniform 1/3 by symmetry. FEM is the only method that stays below 0.5 on every seed; per-pattern MLP requires 7 trained models for the full evidence-pattern set.

Method	seed42	seed43	seed44	seed45	mean \pm std
CEBM ($\lambda=0$)	15.970	17.322	7.676	17.322	14.573 \pm 4.641
MDN ($K_{\text{mix}}=3$)	7.427	12.460	6.596	11.060	9.386 \pm 2.821
FEM shared	0.165	0.314	0.021	0.028	0.132 \pm 0.138
MLP per pattern	0.979	1.011	0.435	0.367	0.698 \pm 0.344

Technical Appendix

Table 8: Per-seed mode-bridge midpoint KL for Experiment 3’s (D , mode-scale) generality grid at $K_X=3$ (2–3 seeds per cell). FEM has lower midpoint KL than CEBM in every cell; the worst absolute FEM KL (~ 4.8) occurs at the $D=10$, $ms=2.0$ corner, consistent with the high- D softmax-gradient saturation regime discussed in Section 7. The $K_X \in \{5, 7\}$ extensions appear in Tables 9 and 10.

D	ms	CEBM raw				FEM raw				ratio (mean)
		seed42	seed43	seed44	mean	seed42	seed43	seed44	mean	
2	1.0	1.44	0.83	2.90	1.73	0.747	0.135	0.088	0.323	5.3 \times
2	1.5	0.66	7.01	n/a	3.84	0.092	0.089	n/a	0.090	42 \times
2	2.0	2.75	13.89	n/a	8.32	0.103	0.004	n/a	0.053	157 \times
5	1.0	12.95	5.80	n/a	9.38	2.138	1.338	n/a	1.738	5.4 \times
5	1.5	16.82	17.32	n/a	17.07	3.956	0.004	n/a	1.980	8.6 \times
5	2.0	17.32	17.32	n/a	17.32	0.003	0.042	n/a	0.022	771 \times
10	1.0	16.05	17.32	n/a	16.69	4.000	2.584	n/a	3.292	5.1 \times
10	1.5	17.32	17.32	n/a	17.32	5.762	2.277	n/a	4.019	4.3 \times
10	2.0	17.32	17.32	n/a	17.32	4.606	5.083	n/a	4.844	3.6 \times

Table 9: Per-seed mode-bridge midpoint KL for Experiment 3’s (D , mode-scale) generality grid at $K_X=5$ (2 seeds per cell). FEM has lower midpoint KL than CEBM in every cell at this K_X . Truth at $y=0$ is uniform $1/5$ by class-layout symmetry.

D	ms	CEBM raw			FEM raw			ratio (mean)
		seed42	seed43	mean	seed42	seed43	mean	
2	1.0	0.15	0.11	0.13	0.055	0.018	0.036	3.6 \times
2	1.5	0.06	0.80	0.43	0.061	0.017	0.039	11 \times
2	2.0	6.28	0.96	3.62	0.015	0.030	0.022	162 \times
5	1.0	6.18	6.02	6.10	1.031	1.221	1.126	5.4 \times
5	1.5	16.24	12.72	14.48	0.359	0.095	0.227	64 \times
5	2.0	17.27	12.98	15.13	0.047	0.039	0.043	348 \times
10	1.0	11.75	10.10	10.93	5.545	3.827	4.686	2.3 \times
10	1.5	15.80	20.50	18.15	0.114	1.130	0.622	29 \times
10	2.0	18.26	20.50	19.38	0.163	0.353	0.258	75 \times

Table 10: Per-seed mode-bridge midpoint KL for Experiment 3’s (D , mode-scale) generality grid at $K_X=7$ (2 seeds per cell). FEM has lower midpoint KL than CEBM in every cell at this K_X . Truth at $y=0$ is uniform $1/7$ by class-layout symmetry.

D	ms	CEBM raw			FEM raw			ratio (mean)
		seed42	seed43	mean	seed42	seed43	mean	
2	1.0	0.09	0.06	0.07	0.017	0.047	0.032	2.2 \times
2	1.5	0.57	0.62	0.59	0.006	0.054	0.030	20 \times
2	2.0	3.34	1.94	2.64	0.017	0.017	0.017	156 \times
5	1.0	1.53	2.23	1.88	0.391	0.216	0.303	6.2 \times
5	1.5	3.10	3.33	3.21	0.921	0.147	0.534	6.0 \times
5	2.0	13.78	4.32	9.05	0.615	0.119	0.367	25 \times
10	1.0	7.54	6.67	7.10	6.915	4.319	5.617	1.3 \times
10	1.5	11.61	14.90	13.25	0.144	2.091	1.117	12 \times
10	2.0	19.55	20.70	20.13	0.195	0.381	0.288	70 \times